SCIENCE CHINA
Information Sciences

• Supplementary File •

Signal processing and energy transformation-based cooperative control for PMSM servo systems

Xiangxiang Meng [1], Jie Zhang [1], Haisheng Yu [2*] & Shubo Wang [3]

[1]*School of Information and Electronic Engineering, Shandong Technology and Business University, Yantai, 264005, China*
[2]*School of Automation, Qingdao University, Qingdao, 266071, China*
[3]*Faculty of Mechanical and Electrical Engineering, Kunming University of Science and Technology, Kunming, 650550, China*

Appendix A Introduction

With the advancement of science and technology, for servo-drive devices, particularly permanent magnet synchronous motor (PMSM) servo systems, in practical applications, ensuring fast response speed, high tracking accuracy, strong robustness, and high safety in high-performance control has consistently been a critical research focus from the perspective of performance requirements [1, 2]. The PMSM servo system is a strongly coupled multi-variable nonlinear system, and which inevitably affected by various uncertainties, such as model parameter uncertainties, friction forces and unknown external load disturbances [3–5]. To reduce these effect of uncertainties on control performance, currently there are mainly kinds of control methods, such that adaptive control [6], robust control [7], and disturbance observer-based control (DOBC) [8–10]. Especially, as a simple and easy to implement anti-disturbance method, DOBC has also been successfully applied to controlled systems in different fields, and has achieved good results in disturbance suppression. For example, underwater robots [11], intelligent transportation [12], and aircraft systems [13, 14]. Besides, the input voltage saturation constraint problem can be regarded as a type of input saturation problem. If the control input exceeds the voltage limit that the inverter can provide, it will cause input voltage saturation constraint, which may lead to negative phenomena such as decreased system control performance or even instability [15, 16]. The consideration of input voltage saturation constraint exacerbates the nonlinear characteristics of PMSM servo systems, further increasing the complexity of controller design. Some scholars solve the input-voltage saturation constraint problem in PMSM servo systems by designing a saturation adaptive optimal control law [17]. A widely used method is to approximate saturation [18] to eliminate nonlinear terms caused by input saturation. However, trajectory tracking, anti-disturbance and input-voltage saturation constraint are interdependent, which may hinder their performance. Therefore, ensuring both trajectory tracking and disturbance suppression under the input-voltage saturation constraint of PMSM servo systems is a challenging problem that deserves further research.

Moreover, from above discussion problem of PMSM servo systems, how to ensure fast response speed, high tracking accuracy, strong robustness and high safety in high-performance control has always been and still is an essential research hotspot from the perspective of performance requirements [19–21]. At present, most PMSM servo systems mainly involve signal processing-based control, which believes that PMSM servo systems are signal processing devices that convert input signals into output signals. The control goal is to quickly reduce or eliminate the trajectory signal (position, velocity, acceleration) errors of the system. The conventional control of trajectory signals in PMSM servo system includes proportional integral (PI) control [22,23], model predictive control [24], backstepping control [25], sliding mode control (SMC) [26, 27], etc. The PI control, as a simple and effective control method, has been widely used in PMSM servo systems to control speed and current. However, in the presence of a wide range of parameter uncertainties and various unknown external disturbances such as unknown sudden loads, using PI controllers cannot achieve satisfactory performances [28]. In [29], the disturbance observer-two-degree of freedom PI controller was proposed to enhance the control performance.

Besides, from the perspective of energy transformation-based control, it is believed that the PMSM servo system is an energy transformation device that converts input energy into output energy, thereby achieving optimization of input energy, output energy and energy dissipation control. In recent years, port-controlled Hamiltonian (PH) [30–32] and passivity-based control [33,34] methods based on the energy transformation control perspective have received high attention. The main feature of PH control methods is that the structure (Hamiltonian or Lagrangian structure) of the closed-loop control system remains unchanged, and its energy (storage) function can be used as a Lyapunov function, making system stability analysis easier, controller design simpler, and practical engineering systems easier to implement. The authors of paper [35] proposed a PH dissipation controller based on interconnect matrix and damping matrix for high precision speed regulation of internal PMSM drivers, but does not consider the influence of parameter perturbation and input saturation.

Signal and energy are two basic concepts, and dynamic systems are generally considered as a unified entity of signal processing and energy transformation with multiple ports (power ports). The PMSM servo system is a nonlinear, multi-variable, strongly coupled, and multi-port signal and energy transformation system. Therefore, only by jointly considering trajectory signal processing and energy transformation, can the essence of the problem be truly revealed by studying the optimization control strategy of the PMSM servo system. The above research is the inspiration for this article. The main contributions of this work are summarized as follows.

* Corresponding author (email: yhsh_qd@qdu.edu.cn)

• A smooth convex combination mechanism-based cooperative control strategy has been designed, fully draws on the advantages of signal processing-based control and energy transformation-based control, simultaneously achieving fast dynamic trajectory signal regulation, accurate trajectory tracking and energy dissipation optimization control.

• The disturbance observer adopts error-based varying gain technique to improve the observation effect, and the control robustness of line and unknown load disturbance variations have also been significantly improved.

• The signal processing-based robust adaptive PI (API) control is adopted to achieve trajectory regulation rapidity at dynamic process. The energy transformation-based adaptive varying damping error-PH (EPH) control is used to achieve energy dissipation optimization control and accurate trajectory tracking at steady-state process.

Appendix B Problem description

In the $d-q$ synchronous rotating coordinate of the PMSM servo system, the form of its dynamic model is expressed as [1–3]

$$\begin{cases} L_{dt}\frac{\mathrm{d}i_d}{\mathrm{d}t} = -R_{st}i_d + n_p\omega L_{qt}i_q + Sat(u_d) + d_{ex1}, \\ L_{qt}\frac{\mathrm{d}i_q}{\mathrm{d}t} = -R_{st}i_q - n_p\omega L_{dt}i_d - n_p\omega\Phi_t + Sat(u_q) + d_{ex2}, \\ \frac{2}{3}J_{mt}\frac{\mathrm{d}\omega}{\mathrm{d}t} = \frac{2}{3}\tau_e + d_{ex3}, \end{cases} \tag{B1}$$

where

• i_d and i_q denote the stator currents in the $d-q$ axis.

• ω represents the mechanical angular velocity of the motor. n_p indicates the number of pole pairs

• u_d and u_q denote the stator voltages in the $d-q$ axis, and $Sat(u_d)$ and $Sat(u_q)$ represent the control input signals with the voltage saturation constraint.

• $L_{dt} = L_d + \Delta L_d$, $L_{qt} = L_q + \Delta L_q$, $J_{mt} = J_m + \Delta J_m$, $\Phi_t = \Phi + \Delta\Phi$, and $R_{st} = R_s + \Delta R_s$ denote the $d-q$ stator inductance, moment of inertia, rotor flux, and the per-phase stator resistance of the motor at run time, respectively.

• ΔL_d, ΔL_q, ΔJ_m, $\Delta\Phi$, and ΔR_s indicate the perturbation variations of the system's nominal parameters L_d, L_q, J_m, Φ, and R_s, respectively.

• τ_f, τ_L, and τ_e ($\tau_e = \frac{3}{2}n_p\{(L_{dt} - L_{qt})i_di_q + \Phi_t i_q\}$) represent the friction torque, load torque, and electromagnetic torque, respectively.

• d_{ex1}, d_{ex2}, and d_{ex3} ($d_{ex3} = -\frac{2}{3}(\tau_f + \tau_L)$) denote the external disturbances.

This article regards the uncertain PMSM servo system with input saturation constraint and unknown external disturbance as a multi-port signal processing and energy transformation device, and establishes its dynamic model as

$$\dot{x} = f(x,p) + gSat(u) + d_{ex}, \tag{B2}$$

where $x = [x_1, x_2, x_3]^{\mathrm{T}} = [L_di_d, L_qi_q, 2/3J_mw]^{\mathrm{T}}$ is the state vector, $f(x,p)$ is n-dimensional smooth vector field with perturbation parameters p, $Sat(u)$ is the control input with voltage saturation constraint, $u = [u_d, u_q]^{\mathrm{T}}$ is the practical control input signal. $d_{ex} = [d_{ex1}, d_{ex2}, d_{ex3}]^{\mathrm{T}}$ is the unknown external disturbances.

Property 1. The control input gain matrix $g \in \mathbb{R}^{n\times m}$, so the generalized inverse matrix of g is described as $g^{\dagger} = \left[g^{\mathrm{T}}g\right]^{-1}g^{\mathrm{T}}$, $m \leqslant n$, $m \in N^+$ and $n \in N^+$.

Property 2. Denote the perturbation parameters be re-described by the constant vector p, and its nominal value is zero. The following property always hold: $f(x,0) = f(x)$.

The input-voltage saturation constraint phenomenon of PMSM servo system can be simply described as

$$Sat_j(u_j) = \begin{cases} u_{\max j}, u_j > u_{\max j} \\ u_j, u_{\min j} \leqslant u_j \leqslant u_{\max j}, \quad j = 1, 2. \\ u_{\min j}, u_j < u_{\min j} \end{cases} \tag{B3}$$

where $u_{\max j}$ and $u_{\min j}$ are known upper and lower bounded of input-voltage saturation constraint respectively.

When the control input signal u_j exceeds the upper limit $u_{\max j}$ or falls below the lower limit $u_{\min j}$, frequent switching of the control signals can lead to chattering, accelerate wear on the mechanical drive components, and undermine the stable performance of the system.

The smooth characterizing function is introduced to approximate above saturation constraint phenomenon in the following form

$$\rho_j(u_j) = u_{Mj} \cdot \mathrm{erf}\left(\frac{\sqrt{\pi}}{2u_{Mj}}u_j\right), \tag{B4}$$

where $u_{Mj} = (u_{\max j} + u_{\min j})/2 + ((u_{\max j} - u_{\min j})/2)\mathrm{sign}(u_j)$, $\mathrm{erf}(x) = \frac{2}{\sqrt{\pi}}\int_0^x \mathrm{e}^{-t^2}\mathrm{d}t$.

Further, the non-smooth saturation phenomenon (B3) is re-expressed as

$$Sat_j(u_j) = \rho_j(u_j) + S_j(u_j), \tag{B5}$$

where $S_j(u_j)$ is an approximation error, it subject bounded $|S_j(u_j)| \leqslant S_{0j}$, S_{0j} is a unknown positive constant and satisfies $S_{0j} = \max\{|u_{\max j} + u_{Mj}|, |u_{\min j} - u_{Mj}|\}$.

The aforementioned problems of model parameter perturbations, unknown external disturbances and input-voltage saturation constraints in PMSM servo system are discussed. Moreover, aiming to achieve fast dynamic trajectory signal regulation, accurate trajectory tracking and optimized energy dissipation control in steady state, we propose a cooperative optimization control scheme based on smooth convex combination mechanism to solve above problems in the following control system design section.

Appendix C Control system design

Consider the smooth saturation function (B4) and the resulting approximation error $S(u)$, (B2) is rewritten as

$$\dot{x} = f(x,p) + g\rho(u) + f_d, \tag{C1}$$

where f_d denotes $f_d = gS(u) + d_{ex}$.

To address the noise impact of measurement signals, the new filtering error variable is introduced as

$$\varepsilon = e + \gamma \int_0^t e\mathrm{d}\tau, \tag{C2}$$

where $e = x - x_0 - \chi$ is the trajectory tracking error, x_0 is the desired trajectory tracking signal of state x, γ is the designed parameter. The χ denotes the auxiliary vector and the following standard auxiliary system-based anti-saturation constraint compensation mechanism (SCCM) is structured to handle input-voltage saturation

$$\dot{\chi} = -\ell\chi + g\Delta u, \tag{C3}$$

where $\Delta u = \rho(u) - u$, $\ell = \mathrm{diag}\{\ell_1, \ell_2, \ell_3\}$, ℓ_i is a designed positive parameter, $i = 1, 2, 3$.

By approximating input-voltage saturation and employing a standard auxiliary system-based anti-saturation constrain compensation mechanism, which can help reduce the impact of input-voltage saturation constrain and is easy to implement in practical applications.

Appendix C.1 Principle and method of cooperative control

This work designs a cooperative control strategy based on trajectory signal control and energy control for PMSM servo system to achieve: i) fast trajectory signal regulation during dynamics period, ii) optimized energy dissipation control and accurate trajectory tracking during steady-state period, iii) continuous smooth changes in control variables during full operation without vibration.

The cooperative control u is composed of a convex combination mechanism of trajectory signal processing-based controller $u_{_S}$ and energy transformation-based controller $u_{_E}$. Then, the convex combination mechanism is designed as

$$gu = C_{_S} gu_{_S} + C_{_E} gu_{_E}, \tag{C4}$$

where $C_{_S} + C_{_E} = I$, I is a unit matrix. $C_{_S} = \mathrm{diag}\{c_{S1}, c_{S2}, c_{S3}\}$ and $C_{_E} = \mathrm{diag}\{c_{E1}, c_{E2}, c_{E3}\}$, c_{Si} and c_{Ei} are the switching functions to be designed. $0 \leqslant c_{Si} \leqslant 1$, $0 \leqslant c_{Ei} \leqslant 1$, $i = 1, 2, 3$. The cooperative control scheme for PMSM servo system is shown in Figure C1.

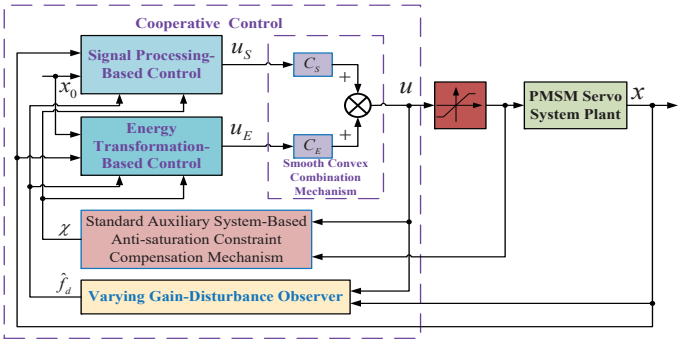

Figure C1 The scheme of cooperative control.

Remark 1. Consider the response of step function signals in both underdamped and overdamped processes as a case study to analyze the working principle of cooperative control based on trajectory error and its rate of change. As depicted in Figure C2 (a), during the underdamped process, although the dynamic response speed of the state trajectory curve obtained using signal processing control is faster than that of other methods, significant overshoot and steady-state errors are observed. Moreover, at points B, C, D and F, while the rate of change of the error is zero, the error itself is not zero. The state trajectory curve using the cooperative control strategy significantly mitigates overshoot and exhibits a faster dynamic response than the energy transformation-based control method. Furthermore, at point E, both the error and its rate of change are zero, indicating that the system has reached steady state. Similarly, as shown in Figure C2 (b), although the error rate at point $\bar{B}$ is zero when using the signal processing-based control method, the error is non-zero, suggesting that the system is still in the dynamic adjustment period. Although the steady-state is achieved at points $\bar{D}$ and $\bar{F}$, a considerable steady-state error remains. In contrast, the state trajectories of the cooperative control strategy and the energy transformation-based control method reach steady state at points $\bar{C}$ and $\bar{E}$, respectively, with both zero error and zero rate of change of

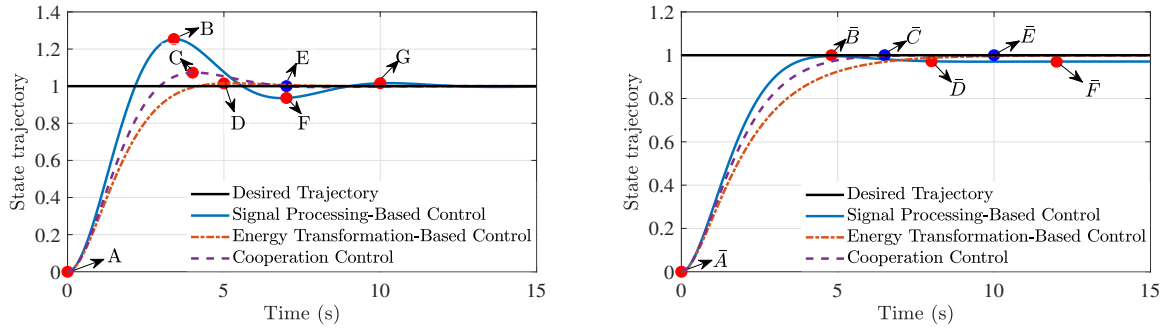

(a) Underdamped process (b) Overdamped process

Figure C2 Response of step function signals with cooperative control.

the error. Furthermore, as observed in the figure, the application of the cooperative control strategy considerably enhances the dynamic response speed relative to the energy transformation-based control method, while eliminating significant steady-state error compared to the signal processing-based control method. Consequently, the cooperative control strategy, which is based on error and its rate of change, is more adept at responding to variations of the system states, enabling rapid trajectory signal adjustment during dynamic processes and precise trajectory tracking during steady-state processes.

Using the direct switching method to design the switching function can cause PMSM servo system to generate shock spikes during operation, reduce the service life of components, and even damage the stability of the entire system. To address this issue, we will design the switching function c_{Si} and c_{Ei} in a smooth and continuous form. Further, introducing trajectory error ε_i and its rate of change $\dot{\varepsilon}_i$ into the smooth switching function enables cooperative control to fully leverage its huge advantages at different stages of system operation. Consider the smooth continuous switching function c_{Si}/c_{Ei} based on the types of linear function, exponential function, and non exponential functions of the trajectory error ε_i and rate of error change $\dot{\varepsilon}_i$. Then, it can be seen from (C4) that through the following comparative study, it is only necessary to determine the error and rate of error change dependent smooth continuous switching function c_{Si}. Design c_{Si} as an exponential function and non-exponential function related to ε_i and $\dot{\varepsilon}_i$, such that Gaussian function C_{SG}, normal distribution function C_{SND}, hyperbolic secant function C_{SHS} and Laplace distribution function C_{SLD}, Cauchy distribution function C_{SCD} and anti-tangent function C_{SAT}.

Table C1 The forms of different functions

Functions	Expression
Gaussian	$c_{SGi} = 1 - \mathrm{e}^{-(\varepsilon_i/\delta_1)^2-(\dot{\varepsilon}_i/\delta_2)^2}$
Normal distribution	$c_{SNDi} = 1 - \frac{1}{\sqrt{2\pi}\delta_i}\mathrm{e}^{-\varepsilon_i{}^2/2\delta_1^2-\dot{\varepsilon}_i^2/2\delta_2^2}$
Hyperbolic secant	$c_{SHSi} = 1 - \frac{2}{\mathrm{e}^{(\varepsilon_i/\delta_1)^2+(\dot{\varepsilon}_i/\delta_2)^2}+\mathrm{e}^{-(\varepsilon_i/\delta_1)^2-(\dot{\varepsilon}_i/\delta_2)^2}}$
Laplace distribution	$c_{SLDi} = 1 - \frac{1}{2\gamma}\exp(-\frac{\lvert\varepsilon_i/\delta_1\rvert+\lvert\dot{\varepsilon}_i/\delta_2\rvert}{\gamma})$
Cauchy distribution	$c_{SCDi} = 1 - \frac{1}{1+\pi((\varepsilon_i/\delta_1)^2+(\dot{\varepsilon}_i/\delta_2)^2)}$
Anti-tangent	$c_{SATi} = \frac{2}{\pi}\arctan((\varepsilon_i/\delta_1)^2 + (\dot{\varepsilon}_i/\delta_2)^2)$

Table C2 The performance comparison results

Functions	$\lvert(\varepsilon_i,\dot{\varepsilon}_i)\rvert \geqslant 1$			$\lvert(\varepsilon_i,\dot{\varepsilon}_i)\rvert < 1$			CC
	RS	AS	SS	RS	AS	SS	
c_{SGi}	fast	high	high	fast	high	high	good
c_{SNDi}	average	high	high	average	low	high	bad
c_{SHSi}	fast	high	high	slow	high	low	average
c_{SLDi}	average	low	high	slow	very low	poor	poor
c_{SCDi}	average	average	high	fast	high	high	average
c_{SATi}	slow	low	high	average	low	high	bad

See from the Figure C3, compared with other continuous function in Table C1, the Gaussian function c_{SGi} has the rapidity of switching (RS), high accuracy of switching (AS), high smooth of switching (SS) and comprehensive comparison (CC), as shown in Table C2. Thus, the smooth continuous switching functions c_{Si} and c_{Ei} are designed as

$$\begin{cases} c_{Si} = 1 - \mathrm{e}^{-(\varepsilon_i/\delta_1)^2-(\dot{\varepsilon}_i/\delta_2)^2}, \\ c_{Ei} = \mathrm{e}^{-(\varepsilon_i/\delta_1)^2-(\dot{\varepsilon}_i/\delta_2)^2}, \end{cases} \tag{C5}$$

where δ_1 and δ_2 are designed scale parameters.

Remark 2. Due to the presence of f_d in $\dot{x}$ in (C1), if the analytical expression of $\dot{\varepsilon}_i$ is directly used, the smooth switching function $c_{Si}(\varepsilon_i, \dot{\varepsilon}_i)$ cannot be used due to its dependence on unknown information. Consider the practical applications, the $\dot{\varepsilon}_i$ do not directly

calculate through this analytical expression (C1). The standard engineering practice we adopt is to obtain the tracking error e and filtering error ε_i from the directly measurable system state x, calculate $\dot{x}$ and $\dot{e}$ using a numerical differentiator, and then obtain the filtering error derivative $\dot{\varepsilon}_i$. By choosing the Gaussian function based on the trajectory error and its rate of change as the smooth convex combination mechanism, the cooperative function between signal processing-based control and energy transformation-based control can be realized more effectively. As $(\varepsilon_i, \dot{\varepsilon}_i) \to \infty$, $c_{Si} \to 1$, $c_{Ei} \to 0$. As $(\varepsilon_i, \dot{\varepsilon}_i) \to 0$, $c_{Si} \to 0$, $c_{Ei} \to 1$. It can be seen from the convex combination mechanism (C4) and (C5) that when the trajectory tracking error is large or the rate of error change is large, signal control plays the main control role and makes the control target converge quickly. When the error and error change rate are small, the energy transformation-based control plays the main control role, and optimizes the input energy, output energy and energy dissipation of PMSM servo system. Moreover, the switching functions c_{Si} and c_{Ei} of (C5) are both smooth and continuous, so convex combination mechanism (C4) can obtain smoothing and continuity performances. Hence, the control variables can also achieve continuous smooth changing during full operation without vibration.

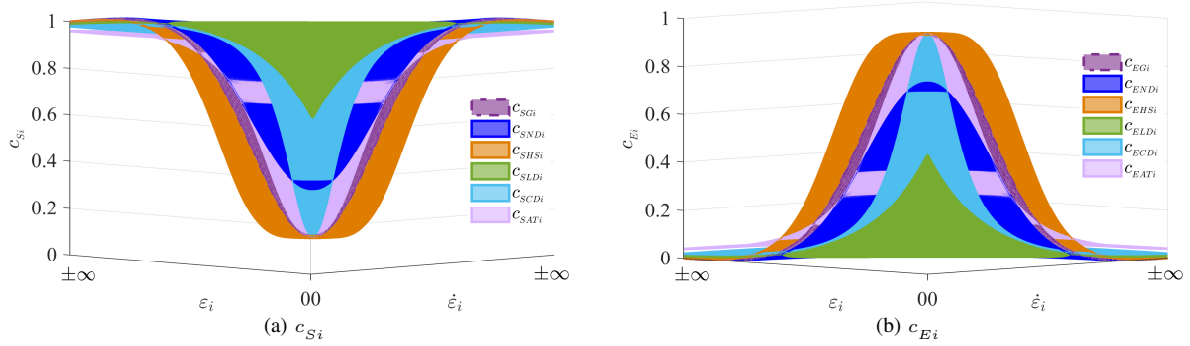

(a) c_{Si} (b) c_{Ei}

Figure C3 The three-dimensional curves of different smooth continuous switching functions with scale parameters $\delta_1 = \delta_2 = 0.5$.

Appendix C.2 Varying gain-disturbance observer

To further improve the system's anti-disturbance performance, a novel varying gain-disturbance observer (VGDO) is designed to estimate the unknown external disturbance f_d and compensate for it in the system. Furthermore, the VGDO serves as a solution to the well-known trade-off between estimation accuracy and transient spikes/noise amplification by high-gain observers.

Assumption 1. The disturbance f_d in the system is differentiable, and its derivatives is considered continuous bounded. The following assumptions always hold that $||\dot{f}_d|| \leqslant \bar{f}_d$, $\bar{f}_d$ is an unknown positive constant.

Assumption 2. The effect of parameter perturbation in the system (C1) can be compensated by the adaptive law designed in the following sections, i.e. $f(x, 0) = f(x)$.

Then, combining with (C1) and (C2), the form of VGDO is constructed as follows

$$\begin{cases} \hat{f}_d = \Xi + \Psi(\varepsilon), \\ \dot{\Xi} = -\hbar\Xi - \hbar(\Psi(\varepsilon) + f(x) + \gamma e - \dot{x}_0 + \ell\chi + gu), \end{cases} \tag{C6}$$

where $\hat{f}_d$ is the estimated vector of disturbances f_d, and Ξ is the auxiliary variables of the designed VGDO.

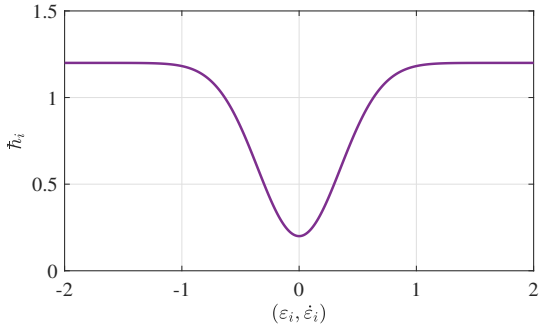

Figure C4 The curve of proposed time-varying gain $\hbar$ when $\hbar_{ci} = 1$ and $\hbar_{mi} = 0.2$.

The nonlinear function $\Psi(\varepsilon)$ and error-based time varying gain matrix $\hbar$ are designed as

$$\begin{cases} \Psi(\varepsilon) = \hbar\varepsilon, \\ \hbar = \hbar_c(\hbar_m + C_S), \end{cases} \tag{C7}$$

where $\hbar = \text{diag}\{\hbar_1, \hbar_2, \hbar_3\}$, $\hbar_c = \text{diag}\{\hbar_{c1}, \hbar_{c2}, \hbar_{c3}\}$ determines the adjustment rate of gain matrix $\hbar$, $\hbar_m = \text{diag}\{\hbar_{m1}, \hbar_{m2}, \hbar_{m3}\}$ determines the minimum gain value of gain matrix $\hbar$, $\hbar_{ci} > 0$, $0 < \hbar_{mi} \leqslant 1$, $0 < \hbar_i \leqslant 2\hbar_{ci}$.

Remark 3. The proposed idea mainly includes two units: fixed unit and time-varying unit. The fixed unit has the gain coefficients ($\hbar_c$, $\hbar_m$) that $\hbar_c\hbar_m$ remains unchanged throughout the whole control process. The time-varying unit has an automatically adjusted time-varying gain that is related to the error and its rate of the change. From Table C2, Figure C3 and Figure C4, one can easy obtain that $\lim\limits_{(\varepsilon_i,\dot{\varepsilon}_i)\to 0}\hbar_i = \hbar_{ci}\hbar_{mi}$, $\lim\limits_{(\varepsilon_i,\dot{\varepsilon}_i)\to \infty}\hbar_i = \hbar_{ci}\hbar_{mi} + \hbar_{ci}$. Therefore, $\hbar_{ci}\hbar_{mi}$ has a strong compensation effect on larger error ε_i and its rate of the change $\dot{\varepsilon}_i$. When ε_i and $\dot{\varepsilon}_i$ decrease, the compensation effect of $\hbar_{ci}\hbar_{mi}$ automatically decreases, in other words, it reduces energy dissipation. In summary, the proposed variable gain technology is primarily used to optimize the performance of the disturbance observer, enabling more accurate estimation and compensation of disturbances in the system. Its effects are reflected in the following aspects: i) Improving disturbance estimation accuracy: By appropriately designing the gain of the disturbance observer, the accuracy of disturbance estimation can be enhanced, enabling the control system to more promptly and accurately detect the presence of disturbances and apply the corresponding compensation. ii) Reducing errors: The error-based variable gain technology helps reduce errors caused by disturbances, particularly in dynamically changing environments. By improving the disturbance estimation accuracy, the disturbance observer can better integrate with the feedback control system, thereby minimizing system errors. iii) Optimizing system response: The error-based variable gain design can also optimize the system's dynamic response while ensuring system stability. For instance, by adjusting the gain based on error, it can improve the system's fast response to disturbances, while avoiding oscillations and instability caused by overcompensation. iv) Reducing impact: Introducing smooth function design for variable gain helps reduce the impact of traditional fixed or switched gains on the system [36,37], and solve the well-known trade-off between estimation accuracy and transient spikes/noise amplification by high-gain observer, thereby enhancing system stability.

Define the disturbance estimation error as $\tilde{f}_d = f_d - \hat{f}_d$, and its estimation error dynamic is expressed as

$$\begin{aligned}\dot{\tilde{f}}_d &= \dot{f}_d - \dot{\hat{f}}_d = \dot{f}_d - \dot{\Xi} - \hbar\dot{\varepsilon}_i \\ &= \dot{f}_d - \{-\hbar\Xi - \hbar(\Psi(\varepsilon) + f(x) + \gamma e - \dot{x}_0 + \ell\chi + gu)\} \\ &\quad - \hbar(f(x) + \gamma e - \dot{x}_0 + \ell\chi + gu + f_d) \\ &= \dot{f}_d - \hbar(f_d - \Xi - \Psi(\varepsilon)) \\ &= \dot{f}_d - \hbar\tilde{f}_d.\end{aligned} \tag{C8}$$

Appendix C.3 Signal processing-based robust API control

This section designs a trajectory signal controller for the PMSM servo system with input-voltage saturation constraints, parameter perturbations and unknown disturbances. The signal processing-based control adopts robust adaptive PI (API) obtain the control target with fast dynamic trajectory signal regulation.

Considering (C2) and (C3), the error dynamic of system (C1) is described as

$$\begin{aligned}\dot{\varepsilon} &= f(x,p) + \gamma e - \dot{x}_0 + \ell\chi + gu_S + f_d \\ &= F(x,p) + \ell\chi + gu_S + f_d,\end{aligned} \tag{C9}$$

where $F(x,p) = f(x,p) + \gamma e - \dot{x}_0$.

Assumption 3. The structure information on $f(x,p)$, γe and x_0 are available to allow an unknown constant vector κ ($\kappa \geqslant 0$), and known function $\varphi(\cdot)$ to be extracted, such that $||F(\cdot)|| \leqslant \kappa\varphi(\cdot)$ for $[0,\infty)$.

Further, the robust API controller is designed as

$$\begin{aligned}u_S &= -g^{\dagger}\{(k_P + \Delta k_p I)e + (k_I + \Delta k_I I)\int_0^t e\mathrm{d}\tau + \ell\chi + \hat{f}_d\} \\ &= -g^{\dagger}\{(k_P + \Delta k_P I)\varepsilon + \ell\chi + \hat{f}_d\},\end{aligned} \tag{C10}$$

where $k_P = \mathrm{diag}\{k_{p1}, k_{p2}, k_{p3}\}$ and $k_I = \gamma k_p$ are designed constant gain matrix. In order to handle the influence of parameter perturbation, the time-varying gains Δk_P and $\Delta k_I = \gamma\Delta k_P$ are introduced by the following adaptive update algorithm

$$\begin{aligned}\Delta k_P &= \hat{\kappa}\varphi, \\ \dot{\hat{\kappa}} &= -\eta_0\hat{\kappa} + \eta_0\varphi\varepsilon^{\mathrm{T}}\Gamma^{-1}C_S\varepsilon,\end{aligned} \tag{C11}$$

where $\hat{\kappa}$ is the estimation of κ, κ being a virtual parameter, and the estimation error is define as $\tilde{\kappa} = \kappa - \hat{\kappa}$. η_0 is positive design parameter, $\varphi = 1 + ||x|| + ||\varepsilon||$.

Remark 4. Compared with traditional PI control, the gain of proposed robust API control consists of constant part and time-varying part. Users can freely choose the values of the constant part, while the time-varying part can automatically and adaptively tune the algorithm continuously. However, the gains of traditional PI control are constants, which require manual adjustment through trial and error. In addition, the proportional gain (k_P, Δk_P) and integral gain (k_I, Δk_I) of proposed robust API control are determined through parameter correlation, rather than being determined independently of each other traditional PI control. This greatly reduces the difficulty of controller parameters tuning. Most importantly, the robust API control can ensure the stability of the system, even in the presence of multisource disturbances and input saturation constraint effects.

Appendix C.4 Energy transformation-based adaptive varying-damping EPH control

This section considers the PMSM servo system as an energy transformation device with multiple ports (power ports). The energy transformation-based control design is constructed by EPH control principle, adaptive and varying-damping techniques to achieve energy dissipation optimization and precise trajectory tracking.

Considering (C1), (C2) and (C3), the following EPH system form is described as

$$\dot{\varepsilon} = \underbrace{(J(\varepsilon,p) - R(\varepsilon,p))\nabla H(\varepsilon,p)}_{F(x,p)+\ell\chi} + g u_{_E} + f_d, \tag{C12}$$

where $H(\varepsilon,p)$ is a bounded continuously and differentiable Hamiltonian storage function, and $\nabla H(\varepsilon,p) = \partial H(\varepsilon,p)/\partial\varepsilon$. $u_{_E}$ is energy control input signal.

By interconnection structure configuring, damping injection and energy shaping of the EPH system, the following objective control is expressed as

$$u_{_E} = v(\varepsilon,p) + v_{\vartheta} + v_d, \tag{C13}$$

where $v(\varepsilon,p)$ is the energy control feedback signal with parameter perturbations, v_{ϑ} is the parameter perturbation compensation adaptive control law, v_d is unknown external disturbances compensation control signal.

Utilizing Property 2, the perturbation of system parameters can be described by a constant vector and its nominal value is usually zero, we obtain that $J(\varepsilon,0) = J(\varepsilon)$, $R(\varepsilon,0) = R(\varepsilon)$, $H(\varepsilon,0) = H(\varepsilon)$ and $v(\varepsilon,0) = v(\varepsilon)$.

Denote a structure matrix $M(\varepsilon)$ of system (C12), and $M(\varepsilon) = J(\varepsilon) - R(\varepsilon)$. $J(\varepsilon)$ is an internal interconnect matrix and it satisfies $J(\varepsilon) = -J^{\mathrm{T}}(\varepsilon) = (M(\varepsilon) - M^{\mathrm{T}}(\varepsilon))/2$, $R(\varepsilon)$ is a damping matrix and it satisfies $R(\varepsilon) = R^{\mathrm{T}}(\varepsilon) = -(M(\varepsilon) + M^{\mathrm{T}}(\varepsilon))/2 \geqslant 0$.

Property 3. The interconnection matrix $J(\varepsilon)$ is an antisymmetric structure that satisfies form $\frac{\partial H^{\mathrm{T}}(\varepsilon)}{\partial\varepsilon} J(\varepsilon) \frac{\partial H(\varepsilon)}{\partial\varepsilon} = 0$. The damping matrix is a symmetric structure that satisfies form $\frac{\partial H^{\mathrm{T}}(\varepsilon)}{\partial\varepsilon} R(\varepsilon) \frac{\partial H(\varepsilon)}{\partial\varepsilon} \geqslant 0$.

Step 1: Interconnection structure configuring and damping injection

The interconnect structure configuring is achieved by introducing a required interconnect structure $J_{_I}(\varepsilon)$, i.e. $J_{_D}(\varepsilon) = J(\varepsilon) + J_{_I}(\varepsilon) = -J_{_D}^{\mathrm{T}}(\varepsilon)$. Damping injection process tuning the desired damping structure $R_{_D}(\varepsilon)$, which is achieved by injecting external damping $R_{_I}(\varepsilon)$, i.e. $R_{_D}(\varepsilon) = R(\varepsilon) + R_{_I}(\varepsilon) = R_{_D}^{\mathrm{T}}(\varepsilon) \geqslant 0$, $R_{_I}(\varepsilon) = \mathrm{diag}\{r_{_{I1}}, r_{_{I2}}, r_{_{I3}}\}$.

With the increasing control requirements, the conventional fixed damping injection technique is difficult to meet. Inspired by the structure of the second-order differential tracker [38], the varying-damping injection mechanism is proposed to be applied to the damping injection stage of EPH, and its form is described as

$$\begin{cases} \dot{\phi}_1 = \phi_2, \\ \dot{\phi}_2 = -\varsigma^2 \left[a_1 \tanh\left(b_1\left(\phi_1 - r(t)\right)\right) - a_2 \tanh\left(b_2\phi_2\right)\right], \\ r_{_{Ii}} = r_d - (r_d - r_s)\,\phi_1, \end{cases} \tag{C14}$$

where $r(t)$ is the virtual input signal, ϕ_1 and ϕ_2 are state vectors, a_1, a_2, b_1, b_2 and ς are designed positive parameters. r_d and r_s are the dynamic state initial value and steady state value of damping injection respectively. By changing the values of the signal $r(t)$, initial damping injection value r_d and damping injection value r_s at steady state, the output curve of the variable $r_{_{Ii}}$ can realize the damping injection for the EPH system with dissipation. For any bounded function $r(t)$ satisfies $\lim\limits_{\varsigma\to\infty} \int_0^{T_0} |\phi_1 - r(t)|\mathrm{d}t = 0 (T_0 > 0)$.

Remark 5. By using a constant large damping injection, the system starts slowly and the dynamic adjustment time is too long. Conversely, a constant small damping injection is used, the dynamic response speed of the system accelerates, but it may lead to significant overshoot phenomena. The proposed varying damping injection mechanism (C14) applies a larger damping value during system starting period to avoid overshoot and improve dynamic performance. During the steady-state process, apply a smaller damping value to ensure steady-state performance and reduce energy loss. Compared with traditional constant injection damping, the proposed varying damping injection mechanism (C14) effectively improves the dynamic and steady-state performance of the system, as well as reduces energy loss.

Step 2: Energy shaping

The energy shaping is simply the addition of energy to the system [35,37], i.e., $H(\varepsilon) \to H_{_D}(\varepsilon)$, and ensure the closed-loop system is stable.

Further, the desired Hamiltonian function $H_{_D}(\varepsilon)$ is constructed as

$$H_{_D}(\varepsilon) = \frac{1}{2}\varepsilon^{\mathrm{T}}\Gamma^{-1}\varepsilon, \tag{C15}$$

where $\Gamma = \mathrm{diag}\{\Gamma_1, \Gamma_2, \Gamma_3\}$, $\Gamma_i > 0$ is the designed parameter. The first-order partial derivative of desired Hamiltonian function $H_{_D}(\varepsilon)$ can be calculated as $\frac{\partial H_{_D}(\varepsilon)}{\partial\varepsilon} = \Gamma^{-1}\varepsilon$.

The perturbation of system parameters can be described by a constant vector and its nominal value is usually zero, but the interconnect structure assignment matrix, desired damping structure and energy shaping are associated with perturbation parameter vector p.

By (C12), interconnection structure configuring, damping injection and energy shaping, the following desired EPH system with dissipation is structured as

$$\dot{\varepsilon} = \left[J_{_D}(\varepsilon,p) - R_{_D}(\varepsilon,p)\right] \frac{\partial H_{_D}(\varepsilon,p)}{\partial\varepsilon} + g v_{\hat{\vartheta}} + \tilde{f}_d. \tag{C16}$$

Decompose functions related to perturbation parameters p, yields

$$\begin{aligned}\frac{\partial H_{D}(\varepsilon,p)}{\partial\varepsilon}&=\frac{\partial H_{D}(\varepsilon)}{\partial\varepsilon}+\Delta_{H}(\varepsilon,p),\\ J_{D}(\varepsilon,p)&=J_{D}(\varepsilon)+\Delta_{J}(\varepsilon,p),\\ R_{D}(\varepsilon,p)&=R_{D}(\varepsilon)+\Delta_{R}(\varepsilon,p),\\ v(\varepsilon,p)&=v(\varepsilon)+\Delta_{v}(\varepsilon,p).\end{aligned}\tag{C17}$$

Considering (C16) and (C17), assuming that function $\psi(\cdot)$ satisfies

$$\left[J_{D}(\varepsilon,p)-R_{D}(\varepsilon,p)\right]\Delta_{H}(\varepsilon,p)-g\Delta_{v}(\varepsilon,p)=g\psi^{\mathrm{T}}\vartheta,\tag{C18}$$

where $\vartheta\in\mathbb{R}^{l}$ is a parameter estimated vector.

Then, the adaptive control law is designed as

$$\begin{cases}v_{\hat{\vartheta}}=-\psi^{\mathrm{T}}\hat{\vartheta},\\ \dot{\hat{\vartheta}}=-\beta\hat{\vartheta}+\beta\psi g^{\mathrm{T}}C_{E}\frac{\partial H_{D}(\varepsilon)}{\partial\varepsilon},\end{cases}\tag{C19}$$

where $\hat{\vartheta}\in\mathbb{R}^{l}$ is the estimated vector of parameter ϑ, β is designed gain parameter.

Therefore, the energy transformation-based adaptive varying-damping EPH control u_{E} is designed as

$$u_{E}=\underbrace{g^{\dagger}\{[J_{D}(\varepsilon)-R_{D}(\varepsilon)]\frac{\partial H_{D}(\varepsilon)}{\partial\varepsilon}-f(x)-\gamma e+\dot{x}_{0}-\ell\chi\}}_{v(\varepsilon)}\underbrace{-g^{\dagger}\hat{f}_{d}}_{v_{d}}\underbrace{-\psi^{\mathrm{T}}\hat{\vartheta}}_{v_{\hat{\vartheta}}}.\tag{C20}$$

Appendix D Stability analysis

Theorem D1. For the system (C1) with Assumptions 1,2, we can choose standard auxiliary system-based anti-saturation constraint compensation mechanism (C3), smooth convex combination mechanism (C4), varying gain-disturbance observer (C6), signal processing-based robust API control (C10) with adaptive update law (C11) and energy transformation-based adaptive varying-damping EPH control (C20) with adaptive update law (C19), so that the error variable ε ultimately converges to a sufficiently small neighborhood of the origin, and all signals ε, $\tilde{\kappa}$, $\tilde{\vartheta}$ and $\tilde{f}_{d}$ in the closed-loop system are uniformly ultimately bounded.

Proof: Choosing a Lyapunov function $V(\varepsilon,\tilde{\kappa},\tilde{\vartheta},\tilde{f}_{d})$ for the system (C1) in the following form

$$V=\frac{1}{2}\varepsilon^{\mathrm{T}}\Gamma^{-1}\varepsilon+\frac{1}{2\eta_{0}}\tilde{\kappa}^{2}+\frac{1}{2\beta}\tilde{\vartheta}^{\mathrm{T}}\tilde{\vartheta}+\frac{1}{2}\tilde{f}_{d}^{\mathrm{T}}\hbar^{-1}\tilde{f}_{d},\tag{D1}$$

where $\tilde{\vartheta}=\vartheta-\hat{\vartheta}$ is denoted parameter estimated error vector.

Taking the derivative of V (D1), yields

$$\begin{aligned}\dot{V}&=\varepsilon^{\mathrm{T}}\Gamma^{-1}\dot{\varepsilon}+\frac{1}{\eta_{0}}\tilde{\kappa}\dot{\tilde{\kappa}}+\frac{1}{\beta}\tilde{\vartheta}^{\mathrm{T}}\dot{\tilde{\vartheta}}+\tilde{f}_{d}^{\mathrm{T}}\hbar^{-1}\dot{\tilde{f}}_{d}\\ &=\varepsilon^{\mathrm{T}}\Gamma^{-1}(f(x,p)+\gamma e-\dot{x}_{0}-\dot{\chi}+g\rho(u)+f_{d})-\frac{1}{\eta_{0}}\tilde{\kappa}(\dot{\kappa}-\dot{\hat{\kappa}})\\ &\quad+\frac{1}{\beta}\tilde{\vartheta}^{\mathrm{T}}(\dot{\vartheta}-\dot{\hat{\vartheta}})+\tilde{f}_{d}^{\mathrm{T}}\hbar^{-1}(\dot{f}_{d}-\hbar\tilde{f}_{d})\\ &=\varepsilon^{\mathrm{T}}\Gamma^{-1}(f(x,p)+\gamma e-\dot{x}_{0}+\ell\chi+gu+f_{d})-\frac{1}{\eta_{0}}\tilde{\kappa}\dot{\hat{\kappa}}\\ &\quad-\frac{1}{\beta}\tilde{\vartheta}^{\mathrm{T}}\dot{\hat{\vartheta}}+\tilde{f}_{d}^{\mathrm{T}}\hbar^{-1}\dot{f}_{d}-\tilde{f}_{d}^{\mathrm{T}}\tilde{f}_{d}\\ &=\varepsilon^{\mathrm{T}}\Gamma^{-1}\{f(x,p)+\gamma e-\dot{x}_{0}+\ell\chi+(C_{S}gu_{S}+C_{E}gu_{E})+f_{d}\}\\ &\quad-\frac{1}{\eta_{0}}\tilde{\kappa}\dot{\hat{\kappa}}-\frac{1}{\beta}\tilde{\vartheta}^{\mathrm{T}}\dot{\hat{\vartheta}}+\tilde{f}_{d}^{\mathrm{T}}\hbar^{-1}\dot{f}_{d}-\tilde{f}_{d}^{\mathrm{T}}\tilde{f}_{d}.\end{aligned}\tag{D2}$$

Since the smooth continuous switch functions C_{S} and C_{E} satisfy $C_{S}+C_{E}=I$, so (D2) can be driven as

$$\begin{aligned}\dot{V}&=\varepsilon^{\mathrm{T}}\Gamma^{-1}\{C_{S}(f(x,p)+\gamma e-\dot{x}_{0}+\ell\chi+gu_{S}+f_{d})\\ &\quad+C_{E}(f(x,p)+\gamma e-\dot{x}_{0}+\ell\chi+gu_{E}+f_{d})\}\\ &\quad-\frac{1}{\eta_{0}}\tilde{\kappa}\dot{\hat{\kappa}}-\frac{1}{\beta}\tilde{\vartheta}^{\mathrm{T}}\dot{\hat{\vartheta}}-\tilde{f}_{d}^{\mathrm{T}}\tilde{f}_{d}+\tilde{f}_{d}^{\mathrm{T}}\hbar^{-1}\dot{f}_{d}.\end{aligned}\tag{D3}$$

Utilizing (C10), (C11) and Assumption 3, we have

$$\begin{aligned}
&\varepsilon^{\mathrm{T}}\Gamma^{-1}\{C_S(f(x,p)+\gamma e-\dot{x}_0+\ell\chi+gu_S+f_d)-\frac{1}{\eta_0}\tilde{\kappa}\dot{\hat{\kappa}}\\
&=\varepsilon^{\mathrm{T}}\Gamma^{-1}C_S\{f(x,p)+\gamma e-\dot{x}_0+\ell\chi-gg^{\dagger}((k_P+\Delta k_P I)\varepsilon+\ell\chi+\hat{f}_d)+f_d\}-\tilde{\kappa}\varphi\varepsilon^{\mathrm{T}}\Gamma^{-1}C_S\varepsilon+\tilde{\kappa}\hat{\kappa}\\
&=\varepsilon^{\mathrm{T}}\Gamma^{-1}C_S\{F(x,p)+\ell\chi-(k_P+\Delta k_P I)\varepsilon-\ell\chi-\hat{f}_d+f_d\}-\tilde{\kappa}\varphi\varepsilon^{\mathrm{T}}\Gamma^{-1}C_S\varepsilon+\tilde{\kappa}\hat{\kappa}\\
&\leqslant-\varepsilon^{\mathrm{T}}\Gamma^{-1}C_S k_P\varepsilon-\hat{\kappa}\varphi\varepsilon^{\mathrm{T}}\Gamma^{-1}C_S\varepsilon-\tilde{\kappa}\varphi\varepsilon^{\mathrm{T}}\Gamma^{-1}C_S\varepsilon+\tilde{\kappa}\hat{\kappa}+\kappa\varphi||\varepsilon^{\mathrm{T}}\Gamma^{-1}C_S||+\varepsilon^{\mathrm{T}}\Gamma^{-1}C_S\tilde{f}_d\\
&\leqslant-\varepsilon^{\mathrm{T}}\Gamma^{-1}C_S k_P\varepsilon+\kappa\varphi\varepsilon^{\mathrm{T}}\Gamma^{-1}C_S\varepsilon-\hat{\kappa}\varphi\varepsilon^{\mathrm{T}}\Gamma^{-1}C_S\varepsilon-\kappa\varphi\varepsilon^{\mathrm{T}}\Gamma^{-1}C_S\varepsilon-\tilde{\kappa}\varphi\varepsilon^{\mathrm{T}}\Gamma^{-1}C_S\varepsilon+\tilde{\kappa}\hat{\kappa}\\
&\quad+\kappa\varphi||\varepsilon^{\mathrm{T}}\Gamma^{-1}C_S||+\varepsilon^{\mathrm{T}}\Gamma^{-1}C_S\tilde{f}_d\\
&\leqslant-\varepsilon^{\mathrm{T}}\Gamma^{-1}C_S k_P\varepsilon-\kappa\varphi\varepsilon^{\mathrm{T}}\Gamma^{-1}C_S\varepsilon+\tilde{\kappa}\hat{\kappa}+\kappa\varphi||\varepsilon^{\mathrm{T}}\Gamma^{-1}C_S||+\varepsilon^{\mathrm{T}}\Gamma^{-1}C_S\tilde{f}_d.
\end{aligned}\tag{D4}$$

Similarly

$$\begin{aligned}
&\varepsilon^{\mathrm{T}}\Gamma^{-1}C_E(f(x,p)+\gamma e-\dot{x}_0+\ell\chi+gu_E+f_d)-\frac{1}{\beta}\tilde{\vartheta}^{\mathrm{T}}\dot{\hat{\vartheta}}\\
&\leqslant\varepsilon^{\mathrm{T}}\Gamma^{-1}C_E\{[J(\varepsilon,p)-R(\varepsilon,p)]\nabla H(\varepsilon,p)+gu_E+f_d\}-\frac{1}{\beta}\tilde{\vartheta}^{\mathrm{T}}\dot{\hat{\vartheta}}\\
&\leqslant\frac{\partial H_D^{\mathrm{T}}(\varepsilon)}{\partial\varepsilon}C_E\{[J_D(\varepsilon,p)-R_D(\varepsilon,p)]\frac{\partial H_D(\varepsilon)}{\partial\varepsilon}+g\psi^{\mathrm{T}}\tilde{\vartheta}+\tilde{f}_d\}\\
&\quad-\tilde{\vartheta}^{\mathrm{T}}\psi g^{\mathrm{T}}C_E\frac{\partial H_D(\varepsilon)}{\partial\varepsilon}-\frac{1}{\beta}\tilde{\vartheta}^{\mathrm{T}}(-\beta\hat{\vartheta}+\beta\psi g^{\mathrm{T}}C_E\frac{\partial H_D(\varepsilon)}{\partial\varepsilon})\\
&\leqslant-\frac{\partial H_D^{\mathrm{T}}(\varepsilon)}{\partial\varepsilon}C_E R_D(\varepsilon,p)\frac{\partial H_D(\varepsilon)}{\partial\varepsilon}+\tilde{\vartheta}^{\mathrm{T}}\hat{\vartheta}+\varepsilon^{\mathrm{T}}\Gamma^{-1}C_E\tilde{f}_d.
\end{aligned}\tag{D5}$$

Combining with the results of (D4) and (D5), (D2) is derived as

$$\begin{aligned}
\dot{V}\leqslant&-\varepsilon^{\mathrm{T}}\Gamma^{-1}C_S k_P\varepsilon-\kappa\varphi\varepsilon^{\mathrm{T}}\Gamma^{-1}C_S\varepsilon-\frac{\partial H_D^{\mathrm{T}}(\varepsilon)}{\partial\varepsilon}C_E R_D(\varepsilon,p)\frac{\partial H_D(\varepsilon)}{\partial\varepsilon}\\
&+\tilde{\kappa}\hat{\kappa}+\kappa\varphi||\varepsilon^{\mathrm{T}}\Gamma^{-1}C_S||+\varepsilon^{\mathrm{T}}\Gamma^{-1}C_S\tilde{f}_d+\tilde{\vartheta}^{\mathrm{T}}\hat{\vartheta}+\varepsilon^{\mathrm{T}}\Gamma^{-1}C_E\tilde{f}_d.
\end{aligned}\tag{D6}$$

Utilizing the Young inequality, one obtains

$$\begin{aligned}
\tilde{\kappa}\hat{\kappa}&\leqslant-\tfrac{1}{2}\tilde{\kappa}^2+\tfrac{1}{2}\kappa^2,\\
\tilde{\vartheta}^{\mathrm{T}}\hat{\vartheta}&\leqslant-\tfrac{1}{2}\tilde{\vartheta}^{\mathrm{T}}\tilde{\vartheta}+\tfrac{1}{2}\vartheta^{\mathrm{T}}\vartheta,\\
\kappa\varphi||\varepsilon^{\mathrm{T}}\Gamma^{-1}C_S||&\leqslant\tfrac{1}{2}\varepsilon^{\mathrm{T}}\Gamma^{-1}\varepsilon+\tfrac{1}{2}\lambda_{\max}(\Gamma^{-1})\kappa^2\varphi^2,\\
\tilde{f}_d^{\mathrm{T}}\hbar^{-1}\dot{f}_d\leqslant\tfrac{1}{2}\tilde{f}_d^{\mathrm{T}}\hbar^{-1}\tilde{f}_d+\tfrac{1}{2}\dot{f}_d^{\mathrm{T}}\hbar^{-1}\dot{f}_d&\leqslant\tfrac{1}{2}\tilde{f}_d^{\mathrm{T}}\hbar^{-1}\tilde{f}_d+\tfrac{1}{2}\lambda_{\max}(\hbar^{-1})\bar{f}_d^2,\\
\varepsilon^{\mathrm{T}}\Gamma^{-1}C_S\tilde{f}_d+\varepsilon^{\mathrm{T}}\Gamma^{-1}C_E\tilde{f}_d=\varepsilon^{\mathrm{T}}\Gamma^{-1}\tilde{f}_d&\leqslant\tfrac{1}{2}\varepsilon^{\mathrm{T}}\Gamma^{-1}\varepsilon+\tfrac{1}{2}\tilde{f}_d^{\mathrm{T}}\Gamma^{-1}\tilde{f}_d.
\end{aligned}\tag{D7}$$

Then, we have

$$\begin{aligned}
\dot{V}&\leqslant-\varepsilon^{\mathrm{T}}\Gamma^{-1}(C_S k_P+C_E R_D(\varepsilon,p)\Gamma^{-1}-I)\varepsilon-\frac{1}{2}\tilde{f}_d^{\mathrm{T}}(2I-\hbar^{-1}-\Gamma^{-1})\tilde{f}_d\\
&\quad-\frac{1}{2}\tilde{\kappa}^2-\frac{1}{2}\tilde{\vartheta}^{\mathrm{T}}\tilde{\vartheta}+\frac{1}{2}\kappa^2+\frac{1}{2}\vartheta^{\mathrm{T}}\vartheta+\frac{1}{2}\lambda_{\max}(\Gamma^{-1})\kappa^2\varphi^2+\frac{1}{2}\lambda_{\max}(\hbar^{-1})\bar{f}_d^2\\
&\leqslant-\lambda_{\min}(C_S k_P+C_E R_D(\varepsilon,p)\Gamma^{-1}-I)\varepsilon^{\mathrm{T}}\Gamma^{-1}\varepsilon-\frac{1}{2}\lambda_{\min}(2\hbar-I-\Gamma^{-1}\hbar)\tilde{f}_d^{\mathrm{T}}\hbar^{-1}\tilde{f}_d\\
&\quad-\frac{1}{2}\tilde{\kappa}^2-\frac{1}{2}\tilde{\vartheta}^{\mathrm{T}}\tilde{\vartheta}+\frac{1}{2}\kappa^2+\frac{1}{2}\vartheta^{\mathrm{T}}\vartheta+\frac{1}{2}\lambda_{\max}(\Gamma^{-1})\kappa^2\varphi^2+\frac{1}{2}\lambda_{\max}(\hbar^{-1})\bar{f}_d^2\\
&\leqslant-\mho_1V(x)+\mho_2.
\end{aligned}\tag{D8}$$

where $\mho_1=\min\{2\lambda_{\min}(C_S k_P+C_E R_D(\varepsilon,p)\Gamma^{-1}-I),\eta_0,\beta,\lambda_{\min}(2\hbar-I-\Gamma^{-1}\hbar)\}$, $\mho_2=\frac{1}{2}\kappa^2+\frac{1}{2}\lambda_{\max}(\Gamma^{-1})\kappa^2\varphi^2+\frac{1}{2}\vartheta^{\mathrm{T}}\vartheta++\frac{1}{2}\lambda_{\max}(\hbar^{-1})\bar{f}_d^2$. By selecting the appropriate parameters, which satisfy $\lambda_{\min}(C_S k_P+C_E R_D(\varepsilon,p)\Gamma^{-1}-I)>0$, $\beta>0$, η_0 and $\lambda_{\min}(2\hbar-I-\Gamma^{-1}\hbar)>0$, i.e. $\mho_1$ and $\mho_2$ are positive definite, $\mho_1>0$, $\mho_2>0$.

Multiplying by $\mathrm{e}^{\mho_1 t}$, yields

$$\mathrm{e}^{\mho_1 t}\dot{V}+\mho_1\mathrm{e}^{\mho_1 t}V\leqslant\mho_2\mathrm{e}^{\mho_1 t}.\tag{D9}$$

Further,

$$0\leqslant V(t)\leqslant(V(0)-\frac{\mho_2}{\mho_1})\mathrm{e}^{-\mho_1 t}+\frac{\mho_2}{\mho_1}\leqslant V(0)+\frac{\mho_2}{\mho_1}.\tag{D10}$$

Based on (D10), we can obtain that V is bounded. Furthermore, considering (D1), (D8), (D10) and the boundedness of V, one can

obtain that ε, $\tilde{\kappa}$, $\tilde{\vartheta}$ and $\tilde{f}_d$ are bounded and hold

$$\begin{aligned}&\lim_{t\to\infty}||\varepsilon||\leqslant\sqrt{\frac{2\lambda_{\min}(C_S k_P+C_E R_D(\varepsilon,p)\Gamma^{-1}-I)\mho_2}{\mho_1}},\quad \lim_{t\to\infty}|\tilde{\kappa}|\leqslant\sqrt{\frac{2\eta_0\mho_2}{\mho_1}},\\&\lim_{t\to\infty}||\tilde{\vartheta}||\leqslant\sqrt{\frac{2\beta\mho_2}{\mho_1}},\quad \lim_{t\to\infty}||\tilde{f}_d||\leqslant\sqrt{\frac{\lambda_{\min}(2\hbar-I-\Gamma^{-1}\hbar)\mho_2}{\mho_1}}.\end{aligned}\tag{D11}$$

and

$$\begin{aligned}&||\varepsilon||\leqslant\sqrt{\frac{2\lambda_{\min}(C_S k_P+C_E R_D(\varepsilon,p)\Gamma^{-1}-I)\mho_2}{\mho_1}+2V(0)},\quad |\tilde{\kappa}|\leqslant\sqrt{\frac{2\eta_0\mho_2}{\mho_1}+2V(0)},\\&||\tilde{\vartheta}||\leqslant\sqrt{\frac{2\beta\mho_2}{\mho_1}+2V(0)},\quad ||\tilde{f}_d||\leqslant\sqrt{\frac{\lambda_{\min}(2\hbar-I-\Gamma^{-1}\hbar)\mho_2}{\mho_1}+2V(0)}.\end{aligned}\tag{D12}$$

Thus, the error variable ε ultimately converges to a sufficiently small neighborhood of the origin, and all signals ε, $\tilde{\kappa}$, $\tilde{\vartheta}$ and $\tilde{f}_d$ in the closed-loop system are uniformly ultimately bounded. Thus, e and also the tracking error are bounded [39, 40]. The proof of Theorem D1 has been completed.

Appendix E Experiment results

Appendix E.1 Experiment plant

The experimental platform and its constituent part of PMSM servo system under proposed cooperative (CO) control strategy are given in Figure E1. This platform consists of computer, 130MB150A salient-free pole PMSM, simulator, servo deriver, motion control card transfer box, and torque sensor of type YH502, etc. The driver (HS0150AE-P22S) used in our experimental system is an HS series servo driver, which uses a digital signal processing (DSP) chip as the core control unit and has universal applicability. By running the Links-RT real time simulation software package, and realize the monitoring of the real time simulator by means of virtual instrument and curve. The control algorithm outputs pulse width modulation waveform through the motor special control card, and collects the encoder value to control the simulator. The experimental platform parameters of PMSM servo system are $L_d = L_q = L = 6.65$mH, $n_p = 4$, $R_s = 1.84\Omega$, $\Phi = 0.32$Wb, $J_m = 0.0027\text{kg}\cdot\text{m}^2$.

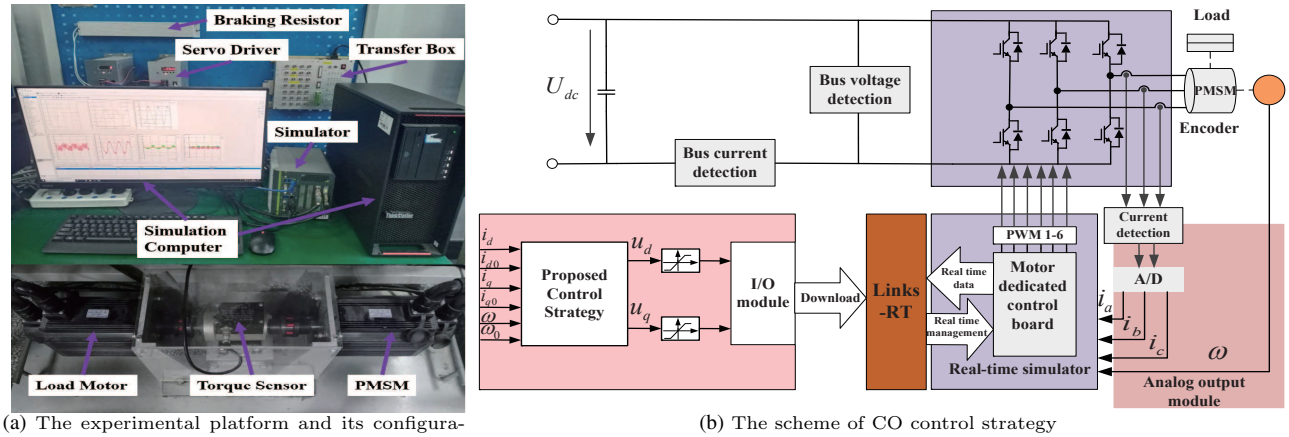

(a) The experimental platform and its configuration

(b) The scheme of CO control strategy

Figure E1 The experimental platform and the proposed CO control scheme for PMSM servo system.

Appendix E.2 Experiment results and discussions

For the compared PI method, the speed controller and current controller are given as below

$$u = k_P\epsilon + k_I\int_0^t \epsilon\mathrm{d}\tau.\tag{E1}$$

where $\epsilon = x - x_0$.

Appendix E.2.1 *Parameters tuning*

Based on the closed-loop analysis results, the controller parameters adjustment meet the following Lyapunov stability requirements of Theorem D1

$$\begin{cases} \eta_0 > 0, \\ \beta > 0, \\ \lambda_{\min}(2\hbar - I - \Gamma^{-1}\hbar) > 0, \\ \lambda_{\min}(C_S k_P + C_E R_D(\varepsilon, p)\Gamma^{-1} - I) > 0. \end{cases} \tag{E2}$$

It means that by selecting the appropriate parameters, which satisfy $\lambda_{\min}(C_S k_P + C_E R_D(\varepsilon, p)\Gamma^{-1} - I) > 0$, $\lambda_{\min}(2\hbar - I - \Gamma^{-1}\hbar) > 0$, $\eta_0 > 0$, $\beta > 0$, i.e. $\mho_1$ and $\mho_2$ are positive definite, $\mho_1 > 0$, $\mho_2 > 0$. The closed-loop system is uniformly ultimately bounded.

The parameter tuning method of proposed CO controller. Taking the varying damping injection parameter regulation of energy transformation-based adaptive varying damping EPH control as an example, discuss the impact of selecting different parameter values on the system. Since the tracking and differentiation components within the integrated control function serve identical roles during operation, we set $a_1 = a_2 = a$ and $b_1 = b_2 = b$, thereby reducing the number of tuning parameters to three. While this reduction in tuning parameters slightly diminishes the degrees of freedom in optimizing the varying-damping parameters, it simplifies the parameter selection process. As illustrated in Figure E2 (a), an increase in the value of parameter ς accelerates the trajectory's convergence speed, but also amplifies noise. Furthermore, as the trajectory approaches stabilization, oscillatory behavior becomes apparent. Figure E2 (b) shows that, with other parameters held constant, increasing parameter a enhances the trajectory's convergence speed. However, if the value of a is too large, oscillations may occur. In Figure E2 (c), with the other parameters fixed, altering parameter b results in faster convergence of the trajectory as the value of b increases. Nevertheless, when $b = 100$, further increases in b have a negligible effect on tracking performance, suggesting that beyond this point, the result of b no longer significantly influences response speed. Thus, the selection of these parameters directly impacts both the convergence speed and the stability characteristics of the trajectory. Consequently, the specific parameter choices should be made based on the desired damping injection transition requirements of the system.

Besides, comparing with traditional PI control, the gain of proposed robust API control consists of constant part and time-varying part. Designers can freely choose the values of the constant part, while the time-varying part can automatically and adaptively tune the algorithm continuously. However, the gains of traditional PI control are constants, which require manual adjustment through trial and error. In addition, in proposed robust API control, the proportional gain (k_P, Δk_P) and integral gain (k_I, Δk_I) are determined through parameter correlation, rather than being determined independently of each other by traditional PI control. Only adjusting the parameters k_P and η_0 are needed, which greatly reduces the difficulty and complexity of parameter tuning.

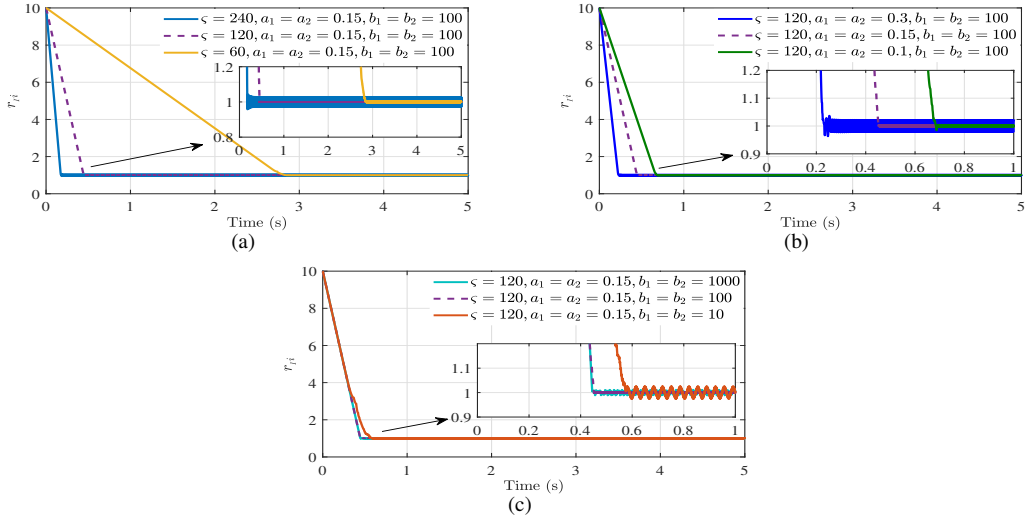

Figure E2 The response curves of varying damping with different parameter values.

Thus, by the above regulation rules, the parameters of proposed CO control are designed as Table E1. The signal processing-based robust API control (C10) and energy transformation-based adaptive varying-damping EPH control (C20) have the same parameters as proposed CO control. The parameters of traditional PI controller (E1) are given that $k_P = \text{diag}\{9, 9, 9\}$, $k_I = \text{diag}\{100, 100, 100\}$.

This work tests the robustness and anti-disturbance of the proposed CO control strategy using unknown external load disturbance changes as an example. The forms of the external load disturbance are assumed as Table E2. In order to effectively and qualitatively evaluate the performance of the proposed CO control strategy, several different performance indicators are used for verification, which include overshoot (OS), time to steady state (TSS), error of steady state (ESS), peak currents/voltages (PC/PV) of q-axis, speed drop/rise (SD/SR), the speed amplitude of chattering (SAC) and recovery time (RT), under several different external load disturbances.

Table E1 Design parameters

Parameters	Values	Parameters	Values
γ	10	ℓ	$\mathrm{diag}\{10, 2000, 50\}$
$\hbar_c$	$\mathrm{diag}\{15, 15, 15\}$	$\hbar_m$	$\mathrm{diag}\{2, 2, 2\}$
k_P	$\mathrm{diag}\{2000, 1800, 10\}$	$\delta_1 = \delta_2$	0.001
Γ^{-1}	$\mathrm{diag}\{L_d, L_q, \frac{2}{3}J_m\}$	η_0	1
β	2	ς	120
r_d	10	r_s	1
$a_1 = a_2$	0.15	$b_1 = b_2$	100

Table E2 The forms of the external load disturbances

Types	Functions	Time Frame
Starting Fixed Load	$\tau_{_L} = 2\mathrm{N}\cdot\mathrm{m}$	$t \in [0, 15]$ s
Sudden Load	$\tau_{_L} = 0\mathrm{N}\cdot\mathrm{m}(\mathrm{nominal})$	$t \in [0, 5)$ s
	$\tau_{_L} = 2\mathrm{N}\cdot\mathrm{m}$	$t \in [5, 10)$ s
	$\tau_{_L} = 0\mathrm{N}\cdot\mathrm{m}$	$t \in [10, 15]$ s
Time-Varying Load	$\tau_{_L} = 0\mathrm{N}\cdot\mathrm{m}(\mathrm{nominal})$	$t \in [0, 5)$ s
	$\tau_{_L} = 0.5\sin(2\pi t) + 0.5\mathrm{N}\cdot\mathrm{m}$	$t \in [5, 10)$ s
	$\tau_{_L} = 0\mathrm{N}\cdot\mathrm{m}$	$t \in [10, 15]$ s

Appendix E.2.2 *Starting fixed load disturbance suppression performance*

Considering the situation that the PMSM servo system operates under external load 2 $\mathrm{N}\cdot\mathrm{m}$ during the starting period, exhibits speed, d-q axis current and voltage response curves by using PI no smooth saturation (PI-NSS), PI, API, EPH and the proposed CO control methods, as shown in Figure E3. It can be seen that the time to steady state of API is shorter than PI-NSS, PI and SMC [27] methods, which is 0.5 s, 0.5 s, 0.2 s and 0.12 s respectively. The error of steady state of PI-NSS, PI, SMC [27], API and EPH is -9/8 rpm, -9/8 rpm, -3/2 rpm, -3/3 rpm and -2/1 rpm, which means the EPH method has better steady state performance than other methods. The proposed CO control method compared with API method has better steady state performance, and has better dynamic performance than EPH method. Especially by PI-NSS, due to the lack of soft starting and smooth saturation treatment, the system experiences significant impulse currents and voltages during the starting period. The use of signal processing-based robust API, energy transformation-based adaptive varying-damping EPH and proposed CO control methods not overshoot phenomena. The performance indicators of different methods under starting fixed load disturbance are compared in Table E3.

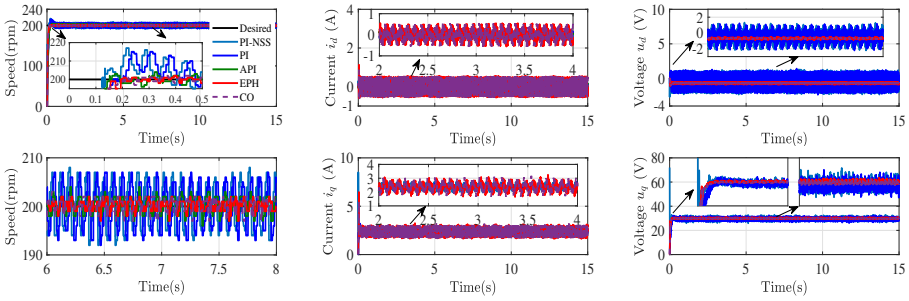

Figure E3 Variable response curves of the PMSM servo system under starting fixed load disturbance using PI-NSS, PI, API, EPH and proposed CO control methods.

Appendix E.2.3 *Sudden load disturbance suppression performance*

Considering the system with an external load of 2 $\mathrm{N}\cdot\mathrm{m}$ at runtime $t = 5$ s. The speed, d-q axis current and voltage response curves of the PMSM servo system by utilizing PI-NSS, PI, SMC [27], API, EPH and the proposed CO control methods are shown in Figure E4. When there is an external load disturbance change, the speed curves controlled by PI-NSS, PI and SMC [27] have the significant drop and rise phenomenon. The response curves of using API, EPH, and CO control methods have the smaller amplitude of drop and rise, the speed response curve fluctuates less, and the recovery time is shorter after adding the external load disturbance, reflecting better disturbance suppression performance. The speed drop/rise of PI-NSS, PI, SMC [27], API, EPH and proposed CO control method is 48/50 rpm, 35/38 rpm, 33/22 rpm, 25/17 rpm, 25/16 rpm and 25/17 rpm. In addition, the proposed CO control strategy compares with [26] (impulse current 7 A), there is no impulse current during the starting period. Compared with [26,27] (0.5 s/0.66 s, 0.15 s/0.15 s), the fluctuation of speed response is smaller during the system subjecting external load disturbance, and the recovery time is shorter. There is no oscillation phenomenon when the external load disturbance changes. The performance indicators of different methods under sudden load disturbance are compared in Table E4.

Table E3 The performance parameters of different methods under starting fixed load disturbance

Methods	Performances				
	TSS(s)	OS(rpm)	ESS(rpm)	PC(A)	PV(V)
PI-NSS	0.5	18	-9/8	8	76
PI	0.5	16	-9/8	3	26
SMC [27]	0.2	8	-3/2	4	/
API	0.12	0	-3/3	3	25
EPH	0.2	0	-2/1	2	25
Proposed CO	0.18	0	-2/2	3	25

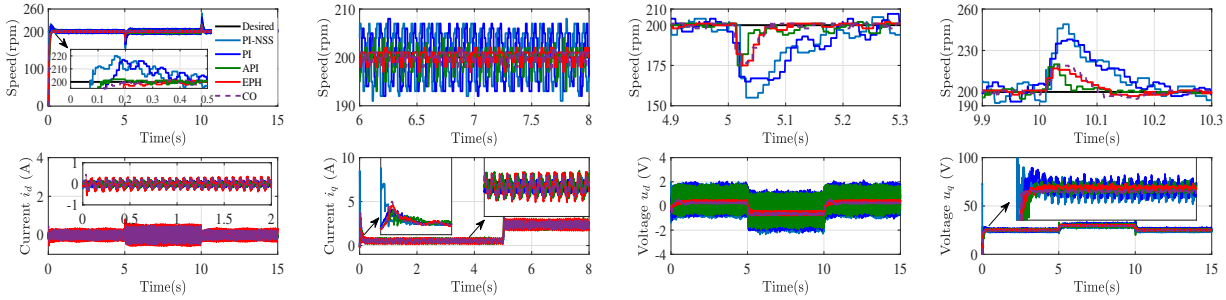

Figure E4 Variable response curves of the PMSM servo system under sudden load disturbance using PI-NSS, PI, API, EPH and proposed CO control methods.

Table E4 The performance parameters of different methods under sudden load disturbance

Methods	Performances				
	TSS(s)	OS(rpm)	SD(rpm)	SR(rpm)	RT(s)
PI-NSS	0.5	20	48	50	0.25/0.25
PI	0.5	17	35	38	0.22/0.25
SMC [26]	0.6	5	35	30	0.5/0.66
SMC [27]	0.2	8	33	22	0.15/0.15
API	0.12	0	25	17	0.07/0.06
EPH	0.2	0	25	16	0.07/0.12
Proposed CO	0.15	0	25	17	0.07/0.1

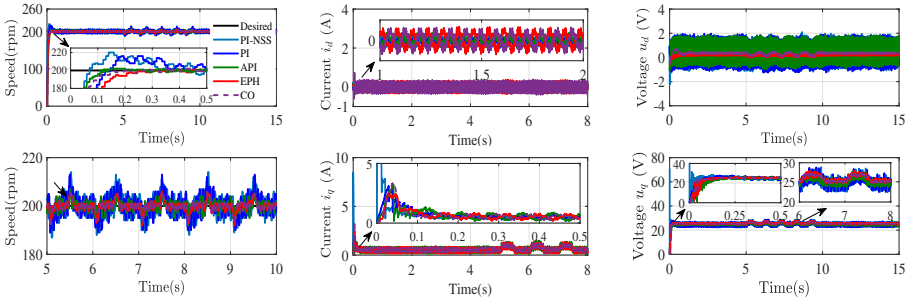

Figure E5 Variable response curves of the PMSM servo system under time-varying load disturbance using PI-NSS, PI, API, EPH and proposed CO control methods.

Table E5 The performance parameters of different methods under time-varying load disturbance

Methods	Performances			
	TSS(s)	OS(rpm)	ESS(rpm)	SAC(rpm)
PI-NSS	0.5	20	-6/6	-15/15
PI	0.5	17	-6/6	-14/14
API	0.12	0	-3/-3	-5/4
EPH	0.2	0	-2/1	-6/6
Proposed CO	0.15	0	-2/1	-5/5

Appendix E.2.4 *Time-varying load disturbance suppression performance*

Consider the time-varying load operation with $0.5\sin(2\pi t) + 0.5$ N · m when the system runs at time $t = 5$ s. The speed, d-q axis current and voltage response curves of the PMSM servo system by using PI-NSS, PI, API, EPH and the proposed CO control methods are shown in Figure E6. After adding external time-varying loads disturbance, there is a significant chattering phenomenon in the speed response curves controlled by PI-NSS and PI. The speed response amplitude under external time-varying loads disturbance of PI-NSS, PI, API, EPH and proposed CO method is -15/15 rpm, -14/14 rpm, -5/4 rpm, -6/6 rpm and -5/5 rpm. The response curves of using API, EPH, and proposed CO control methods have the smaller variation amplitude, reflecting better disturbance suppression performance than other two methods. In addition, the proposed CO control strategy compares with [3], when the system is subjected to external time-varying load disturbance, the fluctuation of current is smaller. The performance indicators of different methods time-varying load disturbance are compared in Table E5.

Appendix E.2.5 *The performance of SCCM*

Maintain the controller parameters unchanged, and consider the impact of the proposed SCCM on the system under sudden disturbance and compare with the proposed method without SCCM. From the experimental results in Figure 10, it can be concluded that there are significant fluctuations in the speed response curve and q-axis voltage response curve during starting period and load disturbance changes without the use of SCCM. According to the experimental comparison results, the proposed SCCM has good saturation suppression and compensation effects during system starting period and load disturbance changes starting period.

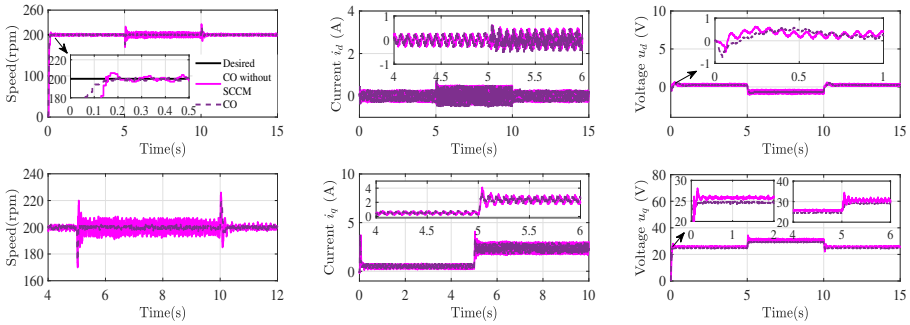

Figure E6 Response curves of the PMSM servo system by proposed CO strategy and without SCCM.

From the above experimental results, we obtain that regardless of the operating conditions of the system, the proposed CO control strategy has smaller steady-state error, more stable current and voltage to PI-NSS, PI and API, and faster dynamic response speed than EPH control. Effectively achieving fast trajectory signal regulation during dynamic operation period, optimizing energy dissipation control and accurate trajectory tracking during steady-state operation period, continuously and smoothly changing control variables of the system during full operation period without vibration, and realizing energy conservation. It is important to note that the proposed CO control strategy introduces a smooth convex combination mechanism (9) to balance the roles of signal processing-based API control and energy transformation-based EPH control. As a result, both methods are active simultaneously during system operation. Therefore, the dynamic response speed of the system using the proposed CO control strategy is slightly slower than that of the signal processing-based control method alone, but it offers higher control accuracy. In comparison with the energy transformation-based adaptive varying-damping EPH control method alone, the control accuracy is slightly lower, but the dynamic response speed is faster.

References

1 S. Li, M. Zhou, and X. Yu, "Design and implementation of terminal sliding mode control method for PMSM speed regulation system," *IEEE Trans. Ind. Inform.*, vol. 9, no. 4, pp. 1879–1891, 2013.
2 H. Du, G. Wen, Y. Cheng, and J. Lü, "Design and implementation of bounded finite-time control algorithm for speed regulation of permanent magnet synchronous motor," *IEEE Trans. Ind. Electron.*, vol. 68, no. 3, pp. 2417–2426, 2021.
3 C. Dai, T. Guo, J. Yang, and S. Li, "A disturbance observer-based current-constrained controller for speed regulation of PMSM systems subject to unmatched disturbances," *IEEE Trans. Ind. Electron.*, vol. 68, no. 1, pp. 767–775, 2021.
4 S. Wang and Q. Chen, "RISE-based prescribed performance control for multimotor driving systems," *IEEE Trans. Ind. Inform.*, vol. 21, no. 7, pp. 5471–5479, 2025.
5 Z. Ping, Y. Jia, B. Xiong, H. Zhang, and J.-G. Lu, "Optimal output regulation for PMSM speed servo system using approximate dynamic programming," *Sci. China-Inf. Sci.*, vol. 66, no. 7, p. 170206, 2023.
6 J. Sun, S. Xu, S. Ding, Z. Pu, and J. Yi, "Adaptive conditional disturbance negation-based nonsmooth-integral control for PMSM drive system," *IEEE-ASME Trans. Mechatron.*, vol. 29, no. 5, pp. 3602–3613, 2024.
7 S. Wang, C. Sun, Q. Chen, and H. He, "Composite learning fixed-time control for nonlinear servo systems with state constraints and unknown dynamics," *IEEE Trans. Syst. Man Cybern. -Syst.*, vol. 55, no. 3, pp. 2332–2342, 2025.
8 J. Yang, W. Chen, S. Li, L. Guo, and Y. Yan, "Disturbance/uncertainty estimation and attenuation techniques in PMSM drives-a survey," *IEEE Trans. Ind. Electron.*, vol. 64, no. 4, pp. 3273–3285, 2017.
9 T. Yang, Y. Du, B. Li, W. Cao, C. Zhang, and J. She, "An enhanced equivalent input disturbance approach to current control of PMSM with periodic and aperiodic disturbances," *Sci. China-Inf. Sci.*, vol. 68, no. 3, p. 132205, 2025.
10 H. Cao, Y. Deng, J. Liu, Y. Zuo, X. Liu, H. Wang, and C. H. Lee, "Improved deadbeat predictive current control of PMSM drives with repetitive control-based disturbance correction observer," *IEEE Trans. Power Electron.*, vol. 40, no. 1, pp. 801–812, 2025.
11 Z. Chu, F. Wang, T. Lei, and C. Luo, "Path planning based on deep reinforcement learning for autonomous underwater vehicles under ocean current disturbance," *IEEE Trans. Intell. Veh.*, vol. 8, no. 1, pp. 108–120, 2023.
12 X. Yao, B. Zhao, X. Li, and S. Li, "Distributed formation control based on disturbance observers for high-speed trains with communication delays," *IEEE Trans. Intell. Transp. Syst.*, vol. 25, no. 5, pp. 3457–3466, 2024.
13 X. Cheng, Z.-W. Liu, H. Hou, and Z.-H. Guan, "Disturbance observer-based nonsingular fixed-time sliding mode tracking control for a quadcopter," *Sci. China-Inf. Sci.*, vol. 65, no. 9, p. 192202, 2022.

14 M. Song, F. Zhang, B. Huang, and P. Huang, "Anti-disturbance control for tethered aircraft system with deferred output constraints," *IEEE-CAA J. Automatica Sin.*, vol. 10, no. 2, pp. 474–485, 2023.
15 G. Feng, C. Lai, W. Li, Z. Li, and N. C. Kar, "Dual reference frame based current harmonic minimization for dual three-phase PMSM considering inverter voltage limit," *IEEE Trans. Power Electron.*, vol. 36, no. 7, pp. 8055–8066, 2020.
16 J. Zhang, W. Ren, and X. M. Sun, "Extended-state-observer-based nonlinear control for PMSM servo systems with current constraints and voltage saturations," *IEEE Trans. Transp. Electrif.*, vol. 10, no. 2, pp. 2713–2726, 2024.
17 L. N. Tan and T. C. Pham, "Optimal tracking control for PMSM with partially unknown dynamics, saturation voltages, torque, and voltage disturbances," *IEEE Trans. Ind. Electron.*, vol. 69, no. 4, pp. 3481–3491, 2022.
18 H. Chen, Y. Liu, L. Liu, S. Tong, and Z. Gao, "Anti-saturation-based adaptive sliding-mode control for active suspension systems with time-varying vertical displacement and speed constraints," *IEEE Trans. Cybern.*, vol. 52, no. 7, pp. 6244–6254, 2022.
19 C. Yang, F. Meng, H. Zhang, J. Zhao, H. Wang, and L. Zhou, "Optimal coordinated control for speed tracking and torque synchronization of rigidly connected dual-motor systems," *IEEE-ASME Trans. Mechatron.*, vol. 28, no. 5, pp. 2609–2620, 2023.
20 X. Meng, H. Yu, J. Zhang, Q. Yang, and C. Fu, "Adaptive fault-tolerant cooperative optimization control for PMSM servo system with input saturation and multisource disturbances," *IEEE Trans. Power Electron.*, vol. 40, no. 5, pp. 6506–6518, 2025.
21 X. Meng, H. Yu, J. Zhang, S. Wang, and Q. Yang, "Fixed time cooperative control for PMSM servo systems with multisource uncertainties and faults," *IEEE Trans. Power Electron.*, vol. 40, no. 11, pp. 16469–16482, 2025.
22 R. Ortega, N. Monshizadeh, P. Monshizadeh, D. Bazylev, and A. Pyrkin, "Permanent magnet synchronous motors are globally asymptotically stabilizable with PI current control," *Automatica*, vol. 98, pp. 296–301, 2018.
23 C. Xia, B. Ji, and Y. Yan, "Smooth speed control for low-speed high-torque permanent-magnet synchronous motor using proportional integral resonant controller," *IEEE Trans. Ind. Electron.*, vol. 62, no. 4, pp. 2123–2134, 2015.
24 Z. Su, X. Sun, G. Lei, M. Yao, and L. Zhang, "Augmented continuous-control-set model predictive current control for dual three-phase PMSM drives," *IEEE-ASME Trans. Mechatron.*, vol. 30, no. 3, pp. 2367–2378, 2025.
25 G. Wang, D. Wang, H. Lin, J. Wang, and X. Yi, "A DC error suppression adaptive second-order backstepping observer for sensorless control of PMSM," *IEEE Trans. Power Electron.*, vol. 39, no. 6, pp. 6664–6676, 2024.
26 X. Guo, S. Huang, K. Lu, Y. Peng, H. Wang, and J. Yang, "A fast sliding mode speed controller for PMSM based on new compound reaching law with improved sliding mode observer," *IEEE Trans. Transp. Electrif.*, vol. 9, no. 2, pp. 2955–2968, 2023.
27 Z. Zhang, X. Liu, J. Yu, and H. Yu, "Time-varying disturbance observer based improved sliding mode single-loop control of PMSM drives with a hybrid reaching law," *IEEE Trans. Energy Convers.*, vol. 38, no. 4, pp. 2539–2549, 2023.
28 A. Apte, U. Thakar, and V. Joshi, "Disturbance observer based speed control of PMSM using fractional order PI controller," *IEEE-CAA J. Automatica Sin.*, vol. 6, no. 1, pp. 316–326, 2019.
29 Y. Fan, J. Chen, Q. Zhang, and M. Cheng, "An improved inertia disturbance suppression method for PMSM based on disturbance observer and two-degree-of-freedom PI controller," *IEEE Trans. Power Electron.*, vol. 38, no. 3, pp. 3590–3599, 2023.
30 P. Borja, R. Ortega, and J. M. Scherpen, "New results on stabilization of port-Hamiltonian systems via PID passivity-based control," *IEEE Trans. Autom. Control*, vol. 66, no. 2, pp. 625–636, 2021.
31 Q. Zhong and M. Stefanello, "A port-Hamiltonian control framework to render a power electronic system passive," *IEEE Trans. Autom. Control*, vol. 67, no. 4, pp. 1960–1965, 2022.
32 C. Lv, Z. Wang, Y. Zhang, J. Chen, and H. Yu, "Cooperative formation control of multiple unmanned surface vessels based on state error port control Hamiltonian framework," *Ocean Eng.*, vol. 313, p. 119410, 2024.
33 J. Liu, Z. Liu, W. Chen, and H. Su, "Passivity-based control for interleaved double dual boost converters in DC microgrids supplying constant power loads," *IEEE Trans. Transp. Electrif.*, vol. 8, no. 2, pp. 1642–1655, 2022.
34 A. Rajeev VK and V. Prasad, "Online adaptive gain for passivity based control for sensorless BLDC motor coupled with DC motor for EV application," *IEEE Trans. Power Electron.*, vol. 38, no. 11, pp. 13625–13634, 2023.
35 M. N. Uddin, Z. Zhai, and I. K. Amin, "Port controlled Hamilton with dissipation-based speed control of IPMSM drive," *IEEE Trans. Power Electron.*, vol. 35, no. 2, pp. 1742–1752, 2020.
36 Y. Wang, H. Yu, and Y. Liu, "Speed-current single-loop control with overcurrent protection for PMSM based on time-varying nonlinear disturbance observer," *IEEE Trans. Ind. Electron.*, vol. 69, no. 1, pp. 179–189, 2022.
37 X. Meng, H. Yu, J. Zhang, and Q. Yang, "Smooth switching mechanism-based adaptive integral terminal SMC for PMSM servo system with stator voltage saturation and unknown disturbances," *Control Theory Technol.*, vol. 23, no. 2, pp. 294–309, 2025.
38 W. Wang and S. Tong, "Adaptive fuzzy bounded control for consensus of multiple strict-feedback nonlinear systems," *IEEE Trans. Cybern.*, vol. 48, no. 2, pp. 522–531, 2017.
39 J. Zhang, W. Ren, and X. Sun, "Current-constrained adaptive robust control for uncertain PMSM drive systems: Theory and experimentation," *IEEE Trans. Transp. Electrif.*, vol. 9, no. 3, pp. 4158–4169, 2023.
40 J. Yang, T. Li, C. Liu, S. Li, and W. Chen, "Nonlinearity estimator-based control of a class of uncertain nonlinear systems," *IEEE Trans. Autom. Control*, vol. 65, no. 5, pp. 2230–2236, 2020.